Progress In Electromagnetics Research C, Vol. 119, 177–190, 2022

Tri-Band Bandpass Filter Using Mixed Short/Open Circuited Stubs and Q-Factor with Controllable Bandwidth for WAS, ISM, and 5G Applications

Omar C. Massamba[1], Pierre Moukala Mpele[1], Franck Moukanda Mbango[1, 2, *], and Désiré Lilonga-Boyenga[1]

Abstract—Designing a multi-band bandpass filter (BPF) with controllable bandwidths is an alternative process to several technologies suggested by researchers. Hence, this paper presents a tri-band BPF in microstrip technology where T-shaped short-and-open stubs have alternating positions to use the maximally flat theory, based on the overall $ABCD$ parameters of the circuit. The combination of the design Q-factor and operating frequency to mismatch the design is the technique basis. The proposed structure comprises quarter wavelength ($\lambda/4$) line section to develop a tri-band BPF frequency. All stubs are symmetrical relative to the center axis, while the prototype has been fabricated on a wafer of $22.42 \times 7.62\,\text{mm}^2$. Using an FR4 HTG-175 with a thickness 1-mm, dielectric constant $\varepsilon_r = 4.4$, and loss tangent $\tan\delta = 0.02$, the (4.06–4.283) GHz, (5.877–6.408) GHz, and (14.281–14.589) GHz are obtained referring to a 10-dB of the return loss. In contrast, the insertion losses at the center frequencies are 2.107/1.354/4.08 dB and the fractional bandwidths of 2.134%, 5.346%, and 8.645%, respectively. This covers WAS (including RLAN), ISM, and 5G applications. However, the attenuation coefficient is between 1.326 dB and 4.368 dB. The tri-band BPF prototype was validated using the Anritsu MS4642B 20 GHz Vector Network Analyzer. The measured and E-simulated results have been compared with good agreement.

1. INTRODUCTION

Several microwave components for communication exchanges have been designed to ease users' lives, and bandpass filter (BPF) plays a crucial role in that device. BPF can be narrow [1–3], wide [4, 5], or ultra-wideband (UWB) [6]. Furthermore, the desire of scientists to lighten the weight and reduce the occupied area of components has led to multi-band microwave devices such as antennas [7, 8] and filters, which became a serious option. Hence, advanced communication systems have an enormous demand for multi-band devices that provide various services at different frequencies [9]. The challenging step in designing filters is to provide innovative structures [10] with at least two notched bands for several applications [11]. These bandpass filters (BPFs) can be dual-bands [12, 13], triple-bands [9, 14], quad-bands [15], and more [16]. There are several ways to design microwave bandpass filters. The literature is large in kinds of configurations. Therefore, there are structures such as microwave photonic filters [17–19], filters with lumped elements [20, 21], mixed lumped components [22], transfer-function (TF) [23, 24], filters with defected ground structure (DGS) [2, 25], multiple mode resonators (MMR) [26–28], spoof surface plasmon polaritons (SSPP) [29], stub loaded resonators (SLR) [30–33], stepped impedance resonators (SIR) [32–34] which can use transmission zeros (TZs) [31] with symmetric [32, 33]

Received 27 January 2022, Accepted 17 March 2022, Scheduled 31 March 2022
* Corresponding author: Franck Moukanda Mbango (franck.moukandambango@umng.cg).
[1] National School of Polytechnic Studies, Electrical and Electronics Engineering Laboratory, Marien Ngouabi University, B.P 69, Brazzaville, Congo. [2] Faculty of Sciences and Techniques, Marien Ngouabi University, B.P 69, Brazzaville, Congo.

or asymmetric structure's geometry [35]. Designers' innovative ideas allowed several filters' shapes such as square [36, 37], T-shapes, L-shapes, and U-shapes [6, 37]. The technology process of fabrication can be in coplanar [38] or microstrip [37, 39] configuration. The use of transmission-lines in the microwave domain for planar circuits can be terminated by open-circuit [40], short-circuit, or mixing configurations [41, 42]. A metallic via (M-via) through one or several substrates [43] that can be crossed (through), blind (hidden) or buried [44] as well-described in [43–45] is often used to connect two different transmission lines or any other structures. In the case of a transmission-line and the ground (GND), this connection represents a short circuit [45].

Some researchers have used short-circuit [4] which is a self through the M-via [46] or open-circuit [47] quarter wavelength stubs ($\lambda/4$) or the mix of both [48]. The transmission line, terminated by short-circuiting [12] or open-circuit configuration, is well-described in [49]. This paper presents mixed open-and-short circuited stubs using the maximally-flat concept [50, 51] to prototype a compact tri-band microwave bandpass filter with an attenuation coefficient of less than 4.5 dB in all covered areas bands. T-shaped cascading stubs constitute the proposed filter topology. That BPF might be used to the Wireless Access Systems (WAS), Industrial, Scientific, Medical (ISM), and the Fifth Generation (5G) bands. The new concept is based on the overall ABCD matrix of the entire structure, obtained by cascading the ABCD matrices of all the involved sections. The design is axially symmetric such as in some filters, using SL-SIR [52], and the BPF quality factor Q is a controllable bandwidth parameter. The Q-factor is also used to mismatch the system at the chosen frequency f_0 and create a notched band. The microstrip technology [53] is used with a mono-layer of FR4 HTG-175 having thickness 1-mm where the dielectric constant $\varepsilon_r = 4.4$ and loss tangent $\tan\delta = 0.02$ [54]. As reported in other works [55], we present results in terms of return loss (RL), insertion loss (IL), attenuation coefficient (AC), fractional bandwidth (FBW), center frequency (CF), and prototype's size surface (S). Two main parts are developed: Section 2 gives the proposed filter's topology and mathematical modeling through the methodology, while the results and discussion are the backbones of Section 3. Finally, a conclusion is made to summarize the advantages and disadvantages of the proposed tri-band bandpass filter.

2. FILTER STRUCTURE AND METHODOLOGY

Without complications, the short-circuited stub technique could provide easy structure and outstanding UWB performance [22], especially when the multi-transmission line sections are quarter-wave ($\lambda/4$) [4]. On the one hand, open-circuited stubs are used to design BPF [56, 57], and on the other hand, open stubs can be used for band-stop filters [58, 59]. Furthermore, the open-circuited stubs can also be quarter-wavelength [60, 61]. Therefore, the proposed filter's topology mixes both configurations with the electric length $\lambda/4$, as shown in Figure 1.

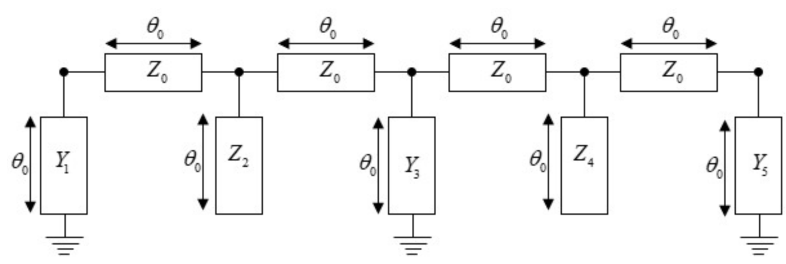

Figure 1. Proposed tri-band BPF with three short-circuited and two open-circuited stubs along with four identical transmission-line sections.

2.1. Topology of the Filter and Principle

Below is the proposed filter, which has four transmission line sections, and five stubs terminated by three short-circuits and two open-circuits.

The transmission line impedance $Z_0 = 50\,\Omega$ and electric length $\theta_0 = \beta l_0$ are computed at a chosen frequency f_0. The design is center axial-symmetrical, appearing at the admittance Y_3. This simplifies

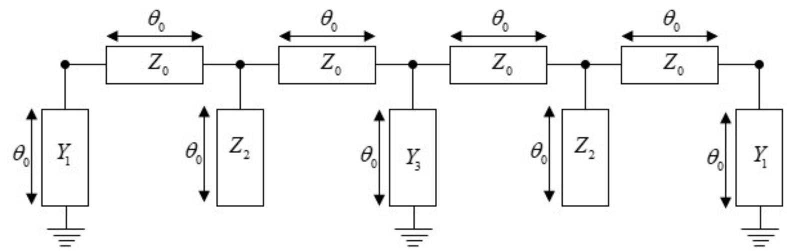

Figure 2. Schematic of the tri-band BPF with pairwise identical short-circuited and open-circuited stubs along with four similar transmission-line sections.

the filter analysis with two conditions: $Y_1 = Y_5$ and $Z_2 = Z_4$. Figure 1 becomes as shown in Figure 2 below.

2.2. Mathematical Modeling: Methodology

From Figure 2, the $ABCD$ matrix of the transmission line (TL) section is given as follows [6],

$$\begin{bmatrix} A_{TL} & B_{TL} \\ C_{TL} & D_{TL} \end{bmatrix} = \begin{bmatrix} \cos\theta_0 & jZ_0 \sin\theta_0 \\ j\sin\theta_0/Z_0 & \cos\theta_0 \end{bmatrix} \tag{1}$$

With $P = -j\cot\theta_0$, and $Y_0 = 1/Z_0$, Equation (1) becomes,

$$\begin{bmatrix} A_{TL} & B_{TL} \\ C_{TL} & D_{TL} \end{bmatrix} = j\sin\theta_0 \begin{bmatrix} P & Z_0 \\ Y_0 & P \end{bmatrix} \tag{2}$$

The quarter-wave of the short-circuited stub is the equivalent of a RLC-parallel circuit, while that becomes a RLC-series circuit for an open-circuited stub. The $ABCD$ matrice of the short-circuited stubs (SC_1) and (SC_3) are written as:

$$\begin{bmatrix} A_{SC_1} & B_{SC_1} \\ C_{SC_1} & D_{SC_1} \end{bmatrix} = \begin{bmatrix} 1 & 0 \\ Y_1 P & 1 \end{bmatrix} \tag{3}$$

$$\begin{bmatrix} A_{SC_3} & B_{SC_3} \\ C_{SC_3} & D_{SC_3} \end{bmatrix} = \begin{bmatrix} 1 & 0 \\ Y_3 P & 1 \end{bmatrix} \tag{4}$$

The open-circuited stub (OC_2) $ABCD$ matrix is given as follows,

$$\begin{bmatrix} A_{OC_2} & B_{OC_2} \\ C_{OC_2} & D_{OC_2} \end{bmatrix} = \begin{bmatrix} 1 & Z_2 P \\ 0 & 1 \end{bmatrix} \tag{5}$$

After calculating the individual $ABCD$ parameter, the overall $ABCD$ parameters of the tri-band BPF are the multiplication of the nine $ABCD$ matrices corresponding to the network (N) in Figure 2. Equations (6)–(8) give the computation of $ABCD$ matrix network step by step as,

$$\begin{bmatrix} A_{N_1} & B_{N_1} \\ C_{N_1} & D_{N_1} \end{bmatrix} = \begin{bmatrix} A_{OC_2} & B_{OC_2} \\ C_{OC_2} & D_{OC_2} \end{bmatrix} \begin{bmatrix} A_{TL} & B_{TL} \\ C_{TL} & D_{TL} \end{bmatrix} \begin{bmatrix} A_{SC_1} & B_{SC_1} \\ C_{SC_1} & D_{SC_1} \end{bmatrix} \tag{6}$$

$$\begin{bmatrix} A_{N_2} & B_{N_2} \\ C_{N_2} & D_{N_2} \end{bmatrix} = \begin{bmatrix} A_{TL} & B_{TL} \\ C_{TL} & D_{TL} \end{bmatrix} \begin{bmatrix} A_{SC_3} & B_{SC_3} \\ C_{SC_3} & D_{SC_3} \end{bmatrix} \begin{bmatrix} A_{TL} & B_{TL} \\ C_{TL} & D_{TL} \end{bmatrix} \tag{7}$$

$$\begin{bmatrix} A_{N_3} & B_{N_3} \\ C_{N_3} & D_{N_3} \end{bmatrix} = \begin{bmatrix} A_{SC_1} & B_{SC_1} \\ C_{SC_1} & D_{SC_1} \end{bmatrix} \begin{bmatrix} A_{TL} & B_{TL} \\ C_{TL} & D_{TL} \end{bmatrix} \begin{bmatrix} A_{OC_2} & B_{OC_2} \\ C_{OC_2} & D_{OC_2} \end{bmatrix} \tag{8}$$

Finally, the overall $ABCD$ parameters (N_T) results are obtained by multiplying Equations (6), (7), and (8) as follows,

$$\begin{bmatrix} A_{N_T} & B_{N_T} \\ C_{N_T} & D_{N_T} \end{bmatrix} = \begin{bmatrix} A_{N_3} & B_{N_3} \\ C_{N_3} & D_{N_3} \end{bmatrix} \begin{bmatrix} A_{N_2} & B_{N_2} \\ C_{N_2} & D_{N_2} \end{bmatrix} \begin{bmatrix} A_{N_1} & B_{N_1} \\ C_{N_1} & D_{N_1} \end{bmatrix} \tag{9}$$

After developing and computing Equation (9), the following results are obtained.

$$\begin{cases} A_{N_T} = 1 + A_2P^2 + A_4P^4 + A_6P^6 + A_8P^8 \\ B_{N_T} = B_1P + B_3P^3 + B_5P^5 + B_7P^7 \\ C_{N_T} = C_1P + C_3P^3 + C_5P^5 + C_7P^7 + C_9P^9 \end{cases} \tag{10}$$

where $A_{N_T} = D_{N_T}$. Each parameter is expressed below,

$$\begin{cases} A_2 = 6 + 4Y_1Z_0 + Z_0Y_3 + 4Y_0Z_2 \\ A_4 = 1 + 4Y_1Z_0 + 4Y_0Z_2 + 2Y_3Z_0 + 2Y_0^2Z_2^2 + 4Y_1Y_3Z_0^2 + 6Y_1Z_2 + 3Y_3Z_2 \\ A_6 = 2Y_1Z_2 + Y_3Z_2 + 2Y_0Y_1Z_2^2 + Y_0Y_3Z_2^2 + 4Y_1Y_3Z_0Z_2 \\ A_8 = Y_1Y_3Z_2^2 \end{cases} \tag{11}$$

$$\begin{cases} B_1 = 4Z_0 \\ B_3 = 4Z_0 + 4Y_3Z_0^2 + 6Z_2 \\ B_5 = 2Z_2 + 4Y_3Z_0Z_2 + 2Y_0Z_2^2 \\ B_7 = Y_3Z_2^2 \end{cases} \tag{12}$$

$$\begin{cases} C_1 = 4Y_0 + 2Y_0^2Z_2 + 2Y_1 + Y_3 \\ C_3 = 4Y_0 + 6Y_0^2Z_2 + 12Y_1 + 2Y_3 + 2Y_0^3Z_2^2 + 8Y_0Y_1Z_2 + 2Y_0Y_3Z_2 + 4Y_1^2Z_0 + 4Y_1Y_3Z_0 \\ C_5 = 2Y_1 + Y_3 + 8Y_0Y_1Z_2 + 2Y_0Y_3Z_2 + 4Y_1^2Z_0 + 4Y_1Y_3Z_0 + 4Y_0^2Y_1Z_2^2 + Y_3Y_0^2Z_2^2 \\ \qquad +6Y_1^2Z_2 + 6Y_1Y_3Z_2 + 4Y_1^2Y_3Z_0^2 \\ C_7 = 2Y_1^2Z_2 + 2Y_1Y_3Z_2 + 2Y_0Y_1^2Z_2^2 + 2Y_0Y_1Y_3Z_2^2 + 4Y_1^2Y_3Z_0Z_2 \\ C_9 = Y_1^2Y_3Z_2^2 \end{cases} \tag{13}$$

The power concepts to $ABCD$ to determine the insertion loss (IL) is given through Equation (14) as follows,

$$\frac{P_g}{P_L} = 1 + \frac{1}{4}\left[(A_{i+1} - D_{i+1})^2 - \left(\frac{B_i}{Z_0} - C_iZ_0\right)^2\right] \tag{14}$$

with P_g the generator power delivered and P_L the power delivered to the load. For the symmetric structure ($A_{N_T} = D_{N_T}$), Equation (14) is written as,

$$\frac{P_g}{P_L} = 1 - \frac{1}{4}\left[\left(\frac{B_i}{Z_0} - C_iZ_0\right)^2\right] \tag{15}$$

Finally, the maximally-flat condition is given by the equation below,

$$B_i = C_iZ_0^2 \tag{16}$$

At the same time, Q_s (for series) and Q_p (for parallel) factors for $\lambda/4$ stubs in short-and open-circuits, as illustrated in Figure 2, are:

$$\begin{cases} Q_p = 2\left\{\dfrac{Q_1\left(Q_3 + \frac{\pi}{4}\right)\left(Q_5 + \frac{\pi}{4}\right)}{2}\right\}^{\frac{1}{3}} \\ Q_s = 2\left\{\dfrac{Q_2\left(Q_4 + \frac{\pi}{4}\right)}{2}\right\}^{-\frac{1}{2}} \end{cases} \tag{17}$$

where

$$\begin{cases} Q_1 = Q_5 = \dfrac{\pi}{8}\dfrac{Y_1}{Y_0} \\ Q_2 = Q_4 = \dfrac{\pi}{8}\dfrac{Z_2}{Z_0} \\ Q_3 = \dfrac{\pi}{8}\dfrac{Y_3}{Y_0} \end{cases} \tag{18}$$

The BPF network quality factor Q_{N_T} is obtained as defined in [62, 63],

$$\frac{1}{Q_{N_T}} = \frac{1}{Q_p} + \frac{1}{Q_s} \tag{19}$$

By substituting Equations (12), (13), and (15) into Eq. (16), developing and solving that, the characteristic impedance Z_2 is determined with Equation (20),

$$Z_2 = \begin{cases} Z_0\left(1 - 2Z_0Y_1\right) \\ \text{or} \\ Z_0\left\{\left(1 - 3Y_1\right) \pm \sqrt{5Z_0Y_1\left(Z_0Y_1 - 2\right)}\right\} \end{cases} \tag{20}$$

and the admittance Y_3 is linked to Z_2 and Y_1 as,

$$Y_3 = \frac{1 + 12Y_1Z_0 + 4Y_1^2Z_0^2 + 2Y_0^2Z_2^2 + 8Y_1Z_2 - Y_0}{4Y_1Z_0^2 - 2Z_0 + 2Z_2} \tag{21}$$

The operating frequency f_0 is taken arbitrarily, and the electric length θ_0 is defined as follows,

$$\theta_0 = 2\pi f_0 \frac{\sqrt{\varepsilon_r}}{c} l_0 \tag{22}$$

and the reference admittance Y_1,

$$Y_1 = 2\pi f_0 X \tag{23}$$

where ε_r is the material dielectric constant, c the vacuum lightspeed velocity, and "X" a random value that the designer must fix to reach the needed goal. The transmission line sections and stub widths are computed by using the empiric mathematical formula, given in Equations (24) and (25),

$$\begin{cases} A = \dfrac{Z_c}{60}\left(\dfrac{\varepsilon_r + 1}{2}\right)^{1/2} + \dfrac{\varepsilon_r - 1}{\varepsilon_r + 1}\left(0.23 + \dfrac{0.11}{\varepsilon_r}\right) \\ w = 8\dfrac{e^A}{e^{(2A)} - 2}h \end{cases} \tag{24}$$

or

$$\begin{cases} B = \dfrac{377\pi}{2Z_c\sqrt{\varepsilon_r}} \\ w = \dfrac{2}{\pi}\left[B - 1 - \ln\left(2B - 1\right) + \dfrac{\varepsilon_r - 1}{2\varepsilon_r}\left\{\ln\left(B - 1\right) + 0.39 - \dfrac{0.61}{\varepsilon_r}\right\}\right]h \end{cases} \tag{25}$$

The following equations give the fractional bandwidth (FBW) and insertion loss (αl) [64],

$$FBW_{(\%)} = 100\left\{2\left(\frac{f_H - f_L}{f_H + f_L}\right)\right\} \tag{26}$$

and,

$$\alpha l_{(\mathrm{dB})} = -S_{21}^{\mathrm{dB}} + S_{11}^{\mathrm{dB}} + 10\log\left\{\frac{1}{\left|S_{11}\right|^2} - 1\right\} \tag{27}$$

where $S_{21}^{(\mathrm{dB})}$ and $S_{11}^{(\mathrm{dB})}$ are the transmission and reflection coefficients, respectively. Equation (27) is for any unmatched system. But if the structure is matched, it becomes as follows,

$$\alpha l_{(\mathrm{dB})} \approx -S_{21}^{\mathrm{dB}} \tag{28}$$

The return loss is defined [65, 66] as below

$$RL_{(\mathrm{dB})} = 10\log\left(\frac{P_{inc}}{P_{ref}}\right) = -S_{11}^{(\mathrm{dB})} \tag{29}$$

while the insertion loss [67] is given as,

$$IL_{(\mathrm{dB})} = 10\log\left(\frac{P_{inc}}{P_t}\right) = -S_{21}^{(\mathrm{dB})} \tag{30}$$

where P_{inc}, P_{ref}, and P_t are the incident, reflected and transmitted power.

3. RESULTS AND DISCUSSION

3.1. Simulated and Measured Results

As stated earlier, we designed, simulated, prototyped, and measured the tri-band BPF device to verify the prediction. The design and layout have been made with the Agilent Design System (ADS) software, while the prototype measurements were done with Anritsu MS4642B 20 GHz VNA. The prototype was manufactured using FR4 HTG-175 with 1 mm thickness, $\varepsilon_r = 4.4$, and $\tan\delta_d = 0.02$. Particular attention is given to all frequency responses at the 10-dB in-band return loss. For $f_0 = 10.7\,\text{GHz}$ and $Q_{ap} = 0.747$, the goal is reached when $X = 402.8e - 15$. Figures 3(a), 3(c), and 3(d) are the fabricated prototype, while Figure 3(b) is the transmission line to be removed from the entire prototype.

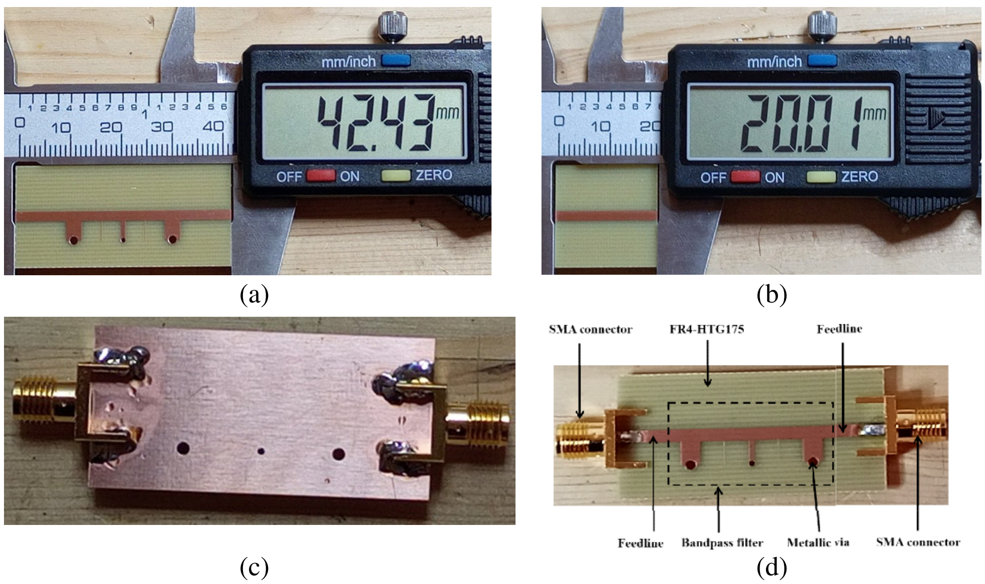

Figure 3. (a) Top view of the prototype. (b) The 20.01-mm microstrip feedline. (c) Bottom view of the fabricated prototype. (d) Prototype's description.

The prototype has been fabricated using the parameters illustrated in Table 1, and all the results are plotted in Figures 4, 5, and 6 coming from that prototype.

Table 1. The manufactured prototype design parameters.

	Resonators 1 & 5: $w_1 = w_5$	Resonators 2 & 4: $w_2 = w_4$	Resonator 3: w_3	Main line: w_0
Impedance (Ω)	36.9272	85.40	76.7518	50
Width (mm)	3.0665	0.1	0.8669	1.9119
Diameter of the via (mm)	1.5	None	0.8	None
Line section's length: l_0 (mm)	3.8086			

On a $170.778\,\text{mm}^2$ of an FR4 wafer, the prototype has been fabricated and occupied $56.673\,\text{mm}^2$. Figure 4 is the prototype results (simulated and measured) in the scanned frequency (3–15) GHz. The results' comparison is made as shown, and a good agreement is noticed through the tendency of measured and simulated data. One transmission zero (TZ) at around 10.7 GHz as desired during the modeling stage is obtained.

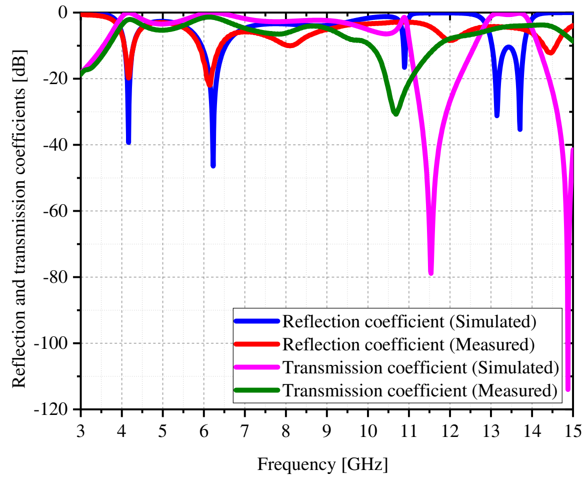

Figure 4. Frequency response (reflection/transmission) measured and simulated (3–15) GHz.

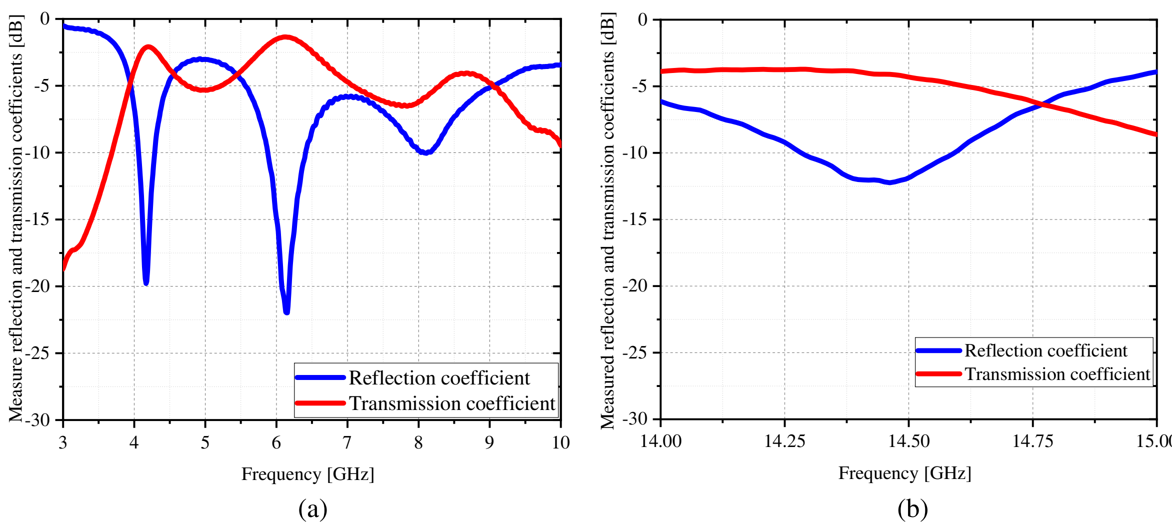

Figure 5. (a) The reflection/transmission coefficient measured in the frequency range (3–10) GHz. (b) The reflection/transmission coefficient measured in the frequency range (14–15) GHz.

By zooming in the different essential parts, plotted in Figure 4, three bandwidths are observed in Figures 5 and 6.

3.2. Results and Discussion

Both Figures 5(a) and 5(b) show three matched bandwidths at 10-dB of the return loss: (4.06–4.283) GHz, (5.877–6.408) GHz, and (14.281–14.589) GHz, which represent an FBW of 5.346%, 8.645%, and 2.134%, respectively, whenEquation (26) is applied. Equations (27) and (28) are consistent with the results found in Figure 6. Table 2 sums up the prototypes' performances.

The AC is between 1.326 dB and 2.466 dB in the two first bandwidths, while it increases in the third bandwidth and does not go over 4.368 dB. The prototype dimensions have been computed at 10.7 GHz to create the mismatched frequency. That is obtained through transmission zero at 10.679 GHz. The theory frequency is close to the experimental frequency found. With a bandwidth of 531 MHz, this developed filter prototype is broadband. At the same time, the designed and fabricated filter is narrowband in its first and third bands. This tri-band BPF is also significant in its return loss parameter

Table 2. The summary of the matched prototype experimental results at RL > 10 dB.

Bandpass filter's Parameters		First Band	Second Band	Third Band
Cut-off frequency (GHz)	f_L	4.06	5.877	14.281
	f_H	4.283	6.408	14.589
Bandwidth (MHz)	Δ	223	531	308
Insertion loss at f_L (dB)	$IL_{(L)}$	2.933	1.958	3.72
Insertion loss at f_H (dB)	$IL_{(H)}$	2.316	2.007	4.819
Attenuation coefficient at f_L (dB)	$\alpha l_{(L)}$	2.466	1.497	3.257
Attenuation coefficient at f_H (dB)	$\alpha l_{(H)}$	1.89	1.558	4.368
Attenuation coefficient at CF (dB)	$\alpha l_{(CF)}$	2.059	1.326	3.799
Transmission zero: f @ S_{21}	10.679 (GHz) @ -30.745 dB			

Table 3. Comparison of the proposed tri-band bandpass filter with state-of-art designs.

Ref.	CF (GHz) @ FBW (%)	Bandwidth (MHz)	RL (dB)	IL (dB)	AC (dB)	Size (mm^2) λ_g^2 @ ε_r	Technology @ year
[9]	6.28 @ 9.5 13 @ 6.2 19.12 @ 4.5	597 806 860	> 13	1.6 2.5 2.2	none	0.26×0.46 @ 2.2	Planar HMSIW + DGS @ 2021
[10]	3.27 @ 3 4.75 @ 2.5 6.3 @ 2.6	98 119 164	> 14	3.23 3.69 1.67	none	0.171×0.143 @ 2.2	CSRR-loaded SIW @ 2012
[16]	0.6 @ 115.2 1.6 @ 37.5 2.55 @ 19.6 3.4 @ 14.4 4.1 @ 10.3 4.6 @ 6.7 5 @ 4.9 5.9 @ 14.4	691 600 500 490 422 308 245 850	> 19	0.1 0.3 0.6 0.3 0.4 0.6 0.5 0.3	none	0.12×0.12 @ 2.65	L-C Lumped optimization @ 2021
[30]	2.3925 @ 1.881 5.255 @ 3.045	45 160	> 20	1.18 1.03	none	0.316×0.126 @ 2.55	SLR @ 2012
[32]	0.91 @ 8 1.81 @ 8.6 2.45 @ 5.4	73 156 132	14.7 15.1 20	1.8 1.36 1.7	none	0.06×0.162	SLSIR @ 2016
[33]	1.8 @ 5.4 3.5 @ 7.3 5.2 @ 8.9	97 255 463	21 17 24	1.84 0.94 1.15	none	0.23×0.23 @ 2.2	SLSIR @ 2017
[36]	4.1 @ 46 8 @ 55	1.886 4.4	15 10	1.2 2.8	none	0.31×0.03 @ 4.4	SLSRR @ 2020
This work	4.1715 @ 5.346 6.1425 @ 8.645 14.435 @ 2.134	223 531 308	19.63 21.98 12.029	2.107 1.354 4.08	2.059 1.326 3.799	0.499×0.169 @ 4.4	Planar cascading T-resonators

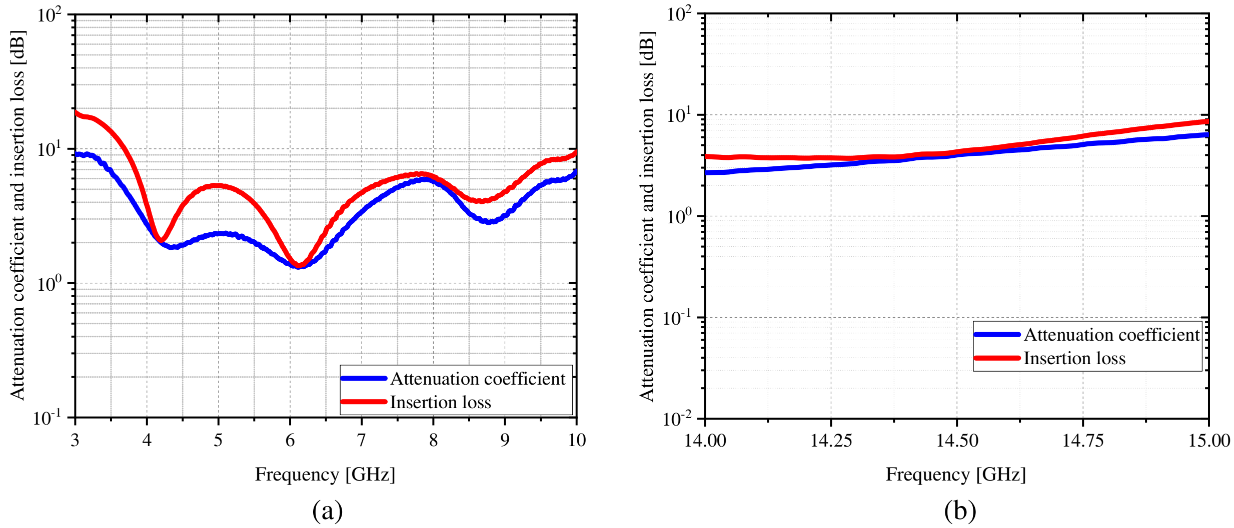

Figure 6. (a) Attenuation/Insertion Loss coefficient measured in the scanned frequency (3–10) GHz. (b) Attenuation/Insertion Loss coefficient measured in the scanned frequency (14–15) GHz.

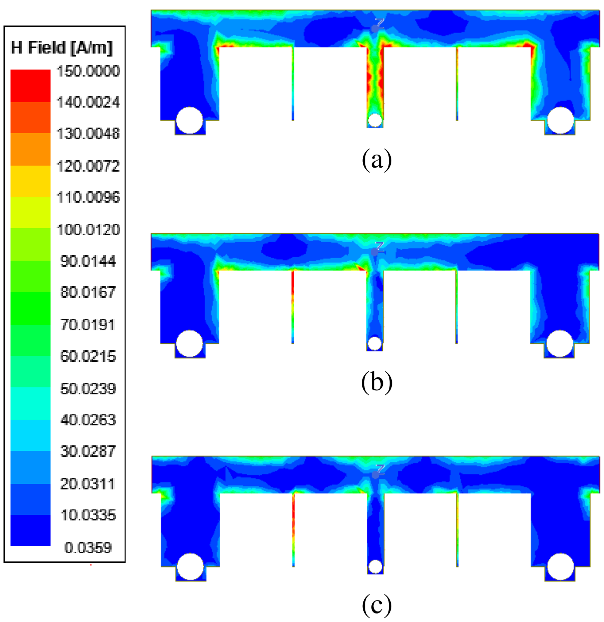

Figure 7. Magnetic field distribution at: (a) 4.1715 GHz, (b) 6.1425 GHz, (c) 14.435 GHz.

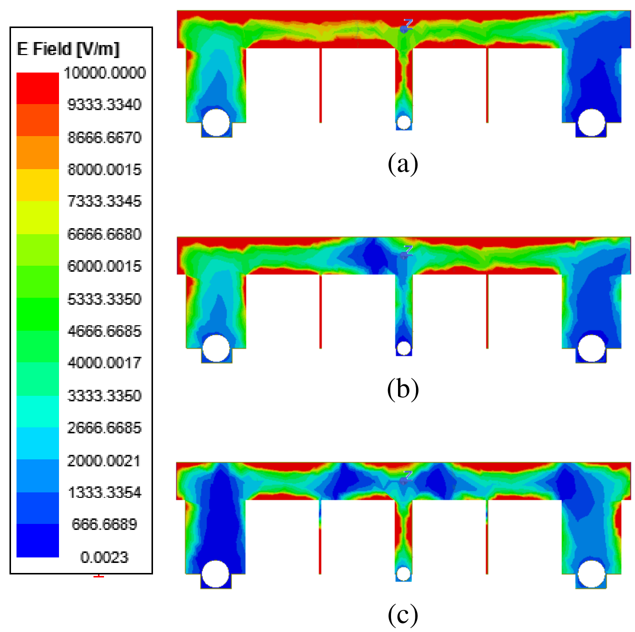

Figure 8. Electrical field distribution at: (a) 4.1715 GHz, (b) 6.1425 GHz, (c) 14.435 GHz.

(19.63 dB, 21.98 dB, and 12.029 dB). The three bands are applied to the WAS, ISM, military and satellite communications, and the 5G bands.

Table 3 denotes that the dielectric choice during the prototype implementation is essential to reducing the circuit's size and losses according to the covering frequency range. Each technology impacts the filter's performance. The proposed tri-band BPF has its simplicity. An easy way to control the bandwidth is to change the Q-factor and the operating frequency f_0 of the main linewidth, calculated to mismatch the design and create two bandwidths before and after that frequency f_0.

3.3. Fields Distribution

The following Figures 7 and 8 show how the H-field and E-Field are distributed in the proposed BPF. It is further verified that the electromagnetic waves are transmitted from the first to the second input. The E-field is well distributed on the mainline and the open-circuited stub, while the H-field is better distributed at the central short-circuited stub.

This distribution depends on the frequency. The lower the frequency is, the higher the fields are distributed.

4. CONCLUSION

This paper has presented an alternative process to fabricate a tri-band bandpass filter (BPF) using the maximally-flat condition. The novelty of the proposed miniaturized tri-band BPF consists of mixing short-and open-circuit stubs using the maximally-flat state. The chosen circuit Q-factor and frequency f_0 are essential in the proposed technique to control the bandwidth and create a notched band. The prototype has been manufactured on an FR4 HTG-175 substrate having a 1-mm thickness. The tri-band BPF has $0.499 \times 0.169\lambda_g^2\,\mathrm{mm}^2$ and was validated with Anritsu MS4642B 20 GHz VNA. $56.673\,\mathrm{mm}^2$ is the proper surface of the tri-band bandpass filter prototype. The waveguide length λ_g was determined at 4.06 GHz for dimensions $22.42 \times 7.62\,\mathrm{mm}^2$. At 10-dB of the return loss, the center frequencies 4.1715/6.1425/14.435 GHz with bandwidths 223/531/308 MHz and the FBWs of 2.134%, 5.346%, and 8.645% have been reached. At the same time, the return loss of 19.63/21.98/12.029 dB and the insertion loss of 2.107/1.354/4.08 dB make it an excellent candidate for the ISM, WAS, and 5G applications. The tri-band bandpass filter was designed using microstrip technology with different cascading T-shape stubs to achieve the cascading chain matrix (CCM) and apply the maximally-flat theory to planar circuits. A short-and-open circuit alternatively terminates those stubs, which are $\lambda/4$ in length. As previously reported, the technology is simple in its implementation, excellent to controllable prototype's bandwidth, and has great performances for integrated systems. For the tri-band BPF implementation, suitable values of Q-factor and f_0 have been chosen to avoid narrow (less than 0.1 mm) or too broad (more than 3.5 mm) linewidth. The measurement and E-simulated results showed an excellent agreement to support the method. Finally, the proposed BPF is both narrowband and broadband.

ACKNOWLEDGMENT

The authors thank the anonymous reviewers for their excellent contributions through the relevant criticisms to improve this work. Grateful acknowledgment is made to PHELINE Laboratory for support during the prototype validation process.

REFERENCES

1. Basavaraju, D. R., H. V. Kumaraswamy, and M. Kothari, "Design and simulation of microstrip narrow band pass filter for Asian Pacific Telecommunication band 28," *RTEICT 2017 — 2nd IEEE International Conference on Recent Trends in Electronics, Information and Communication Technology, Proceedings*, 1313–1316, 2017, doi: 10.1109/RTEICT.2017.8256811.
2. Kumar, A., K. Goodwill, A. K. Arya, and M. V. Kartikeyan, "A compact narrow band microstrip bandpass filter with defected ground structure (DGS)," *IEEE 2012 National Conference on Communications, NCC 2012*, 2–5, 2012, doi: 10.1109/NCC.2012.6176815.
3. Praludi, T., Y. Sulaeman, D. Kurniawan, and I. Syamsu, "Narrow-band microwave planar filter using multiple-poled hairpin resonators," *AIP Conference Proceedings*, Vol. 1755, 1–6, 2016, doi: 10.1063/1.4958606.
4. Wu, Q. S. and L. Zhu, "Wideband impedance transformers with good frequency selectivity based on multisection quarter-wave lines and short-circuited stubs," *IEEE Microwave and Wireless Components Letters*, Vol. 26, 337–339, 2016, doi: 10.1109/LMWC.2016.2548986.

5. Zhang, R. and L. Zhu, "Synthesis design of a wideband bandpass filter with inductively coupled short-circuited multi-mode resonator," *IEEE Microwave and Wireless Components Letters*, Vol. 22, 509–511, 2012, doi: 10.1109/LMWC.2012.2218096.
6. Wang, X., Z. Ma, T. Xie, M. Ohira, C. P. Chen, and G. Lu, "Synthesis theory of ultra-wideband bandpass transformer and its Wilkinson power divider application with perfect in-band reflection/isolation," *IEEE Transactions on Microwave Theory and Techniques*, Vol. 67, 3377–3390, 2019, doi: 10.1109/TMTT.2019.2918539.
7. Moukala Mpele, P., F. Moukanda Mbango, D. B. Onyango Konditi, and F. Ndagijimana, "A tri-band and miniaturized planar antenna based on countersink and defected ground structure techniques," *International Journal of RF and Microwave Computer-Aided Engineering*, Vol. 31, e22617, 2021, doi: 10.1002/mmce.22617.
8. Lakpo, C., F. Moukanda Mbango, D. Bernard, O. Konditi, and P. Moukala Mpele, "A compact dual-band Dolly-shaped antenna with parasitic elements for automotive radar and 5G applications," *Heliyon*, Vol. 7, e06793, 2021, doi: 10.1016/j.heliyon.2021.e06793.
9. Pelluri, S. and M. V. Kartikeyan, "Compact triple-band bandpass filter using multi-mode HMSIW cavity and half-mode DGS," *International Journal of Microwave and Wireless Technologies*, Vol. 13, 103–110, 2021, doi: 10.1017/S1759078720000902.
10. Dong, Y., C. T. M. Wu, and T. Itoh, "Miniaturised multi-band substrate integrated waveguide filters using complementary split-ring resonators," *IET Microwaves, Antennas and Propagation*, Vol. 6, 611–620, 2012, doi: 10.1049/iet-map.2011.0448.
11. Mousavi, O., A. R. Eskandari, M. M. R. Kashani, and M. A. Shameli, "Compact uwb bandpass filter with two notched bands using sislr and DMS structure," *Progress In Electromagnetics Research M*, Vol. 80, 193–201, 2019.
12. Yoon, K. and K. Kim, "Design of dual ultra-wideband band-pass filter using stepped impedance resonator $\lambda g/4$ short stubs and T-shaped band-stop filter," *Electronics*, Vol. 10, 1–10, 2021, doi: 10.3390/electronics10161951.
13. Oudaya Coumar, S. and S. Tamilselvan, "A compact conductor-backed CPW-based dual bandpass filter for satellite S-band and C-band," *Journal of Electrical Systems and Information Technology*, Vol. 7, 2020, doi: 10.1186/s43067-020-00013-8.
14. Wu, Y., E. Fourn, P. Besnier, and C. Quendo, "Direct synthesis of multiband bandpass filters with generalized frequency transformation methods," *IEEE Transactions on Microwave Theory and Techniques*, Vol. 69, 3820–3831, 2021, doi: 10.1109/TMTT.2021.3086835.
15. Cao, Q., H. Liu, and L. Gao, "Design of novel compact quad-band bandpass filter with high selectivity," *Frequenz*, Vol. 74, 53–59, 2020, doi: 10.1515/freq-2019-0043.
16. Yang, Q., S. Liu, K.-D. Xu, and A. Zhang, "Compact octa-band bandpass filter based on controllable transmission zeros with wide upper stopband," *ACES Journal*, Vol. 36, 1159–1163, 2021, doi: 10.47037/2021.ACES.J.360906.
17. Fok, M. P. and J. Ge, "Tunable multiband microwave photonic filters," *Photonics*, Vol. 4, 1–20, 2017, doi: 10.3390/photonics4040045.
18. Liu, Q., J. Ge, and M. P. Fok, "Microwave photonic multiband filter with independently tunable passband spectral properties," *Optics Letters*, Vol. 43, 5685, 2018, doi: 10.1364/ol.43.005685.
19. Ge, J. and M. P. Fok, "Reconfigurable RF multiband filter with widely tunable passbands based on cascaded optical interferometric filters," *Journal of Lightwave Technology*, Vol. 36, 2933–2940, 2018, doi: 10.1109/JLT.2018.2828327.
20. Yildiz, S., A. Aksen, S. Kilinc, and S. B. Yarman, "Multiband filter design using generalized mapping functions and synthesis with lumped resonators," *Radioengineering*, Vol. 29, 343–352, 2020, doi: 10.13164/RE.2020.0343.
21. Miljanović, D., M. Potrebić, and D. V. Tošić, "Design of microwave multibandpass filters with quasilumped resonators," *Mathematical Problems in Engineering*, Vol. 2015, 1–15, 2014, doi: 10.1155/2015/647302.

22. Levy, R., "A new class of distributed prototype filters with applications to mixed lumped/distributed component design," *IEEE Transactions on Microwave Theory and Techniques*, Vol. 18, 1064–1071, 1970, doi: 10.1109/TMTT.1970.1127412.
23. Simpson, D. J., R. Gomez-Garcia, and D. Psychogiou, "Single-/multi-band bandpass filters and duplexers with fully reconfigurable transfer-function characteristics," *IEEE Transactions on Microwave Theory and Techniques*, Vol. 67, 1854–1869, 2019, doi: 10.1109/TMTT.2019.2899849.
24. Simpson, D., R. Gomez-Garcia, and D. Psychogiou, "Multi-band bandpass filters with multiple levels of transfer-function reconfigurability," *Proceedings of the IEEE MTT-S International Microwave Symposium Digest*, 91–94, 2019, doi: 10.1109/mwsym.2019.8700848.
25. Oudaya Coumar, S., "Miniaturized DGS based multi-band pass filters for satellite applications," *Journal of Ambient Intelligence and Humanized Computing*, 1–9, 2021, doi: 10.1007/s12652-021-02898-3.
26. Sengupta, A., S. R. Choudhury, and S. Das, "Super wide band tunable microstrip BPF using stub loaded MMR," *Applied Computational Electromagnetics Society Journal*, Vol. 34, 1399–1404, 2019.
27. Guo, X., Y. Xu, and W. Wang, "Miniaturized planar ultra-wideband bandpass filter with notched band," *Journal of Computer and Communications*, Vol. 3, 100–105, 2015, doi: 10.4236/jcc.2015.33017.
28. Ma, P., B. Wei, J. Hong, Z. Xu, X. Guo, B. Cao, and L. Jiang, "A design method of multimode multiband bandpass filters," *IEEE Transactions on Microwave Theory and Techniques*, Vol. 66, 2791–2799, 2018, doi: 10.1109/TMTT.2018.2815682.
29. Jaiswal, R. K. and N. P. Pathak, "Development and design of multi-band bandpass filter based on the concept of spoof surface plasmon polaritons," *Proceedings of the 11th International Conference on Industrial and Information Systems, ICIIS 2016*, 529–533, 2016, doi: 10.1109/ICIINFS.2016.8262997.
30. Chen, F. C. and J. M. Qiu, "Dual-band bandpass filter with controllable characteristics using stub-loaded resonators," *Progress In Electromagnetics Research Letters*, Vol. 28, 45–51, 2012.
31. Chen, H., X. Wang, and G. Lu, "A Compact bandpass filter with multi-reflection zeros and sharp attenuations," *Proceedings of the 2020 Cross Strait Radio Science and Wireless Technology Conference, CSRSWTC 2020 — Proceedings*, 16–18, 2020, doi: 10.1109/CSRSWTC50769.2020.9372700.
32. Xu, J., "Compact microstrip tri-band bandpass filter using new stubs loaded stepped-impedance resonator," *IEEE Microwave and Wireless Components Letters*, Vol. 26, 249–251, 2016, doi: 10.1109/LMWC.2016.2537740.
33. Li, W., G. Wu, and X. Zhang, "Tri-band bandpass filter using modified tri-section and stub-loaded stepped impedance resonators," *IEICE Electronics Express*, Vol. 14, 1–6, 2017, doi: 10.1049/el.2012.0118.
34. Firmansyah, T., M. Alaydrus, Y. Wahyu, E. T. Rahardjo, and G. Wibisono, "A highly independent multiband bandpass filter using a multi-coupled line stub-sir with folding structure," *IEEE Access*, Vol. 8, 83009–83026, 2020, doi: 10.1109/ACCESS.2020.2989370.
35. Chen, W. Y., M. H. Weng, S. J. Chang, H. Kuan, and Y. H. Su, "A new tri-band bandpass filter for GSM, Wimax and ultra-wideband responses by using asymmetric stepped impedance resonators," *Progress In Electromagnetics Research*, Vol. 124, 365–381, 2012.
36. Zhang, P., L. Liu, D. Chen, M. H. Weng, and R. Y. Yang, "Application of a stub-loaded square ring resonator for wideband bandpass filter design," *Electronics*, Vol. 9, 1–14, 2020, doi: 10.3390/electronics9010176.
37. Thirumalaivasan, K., R. Nakkeeran, and S. Oudaya, "Circular resonator based compact ultra-wideband bandpass and notched filters with rejection of 5–6 GHz band," *Proceedings of the Int. Conf. on Control. Communication and Power Engineering*, 5–8, 2010.
38. Alnahwi, F. M., Y. I. A. Al-Yasir, A. A. Abdulhameed, A. S. Abdullah, and R. A. Abd-Alhameed, "A low-cost microwave filter with improved passband and stopband characteristics using stub loaded multiple mode resonator for 5G mid-band applications," *Electronics*, Vol. 10, 1–15, 2021, doi: 10.3390/electronics10040450.

39. Mohyuddin, W., G. H. Lee, D. S. Woo, H. C. Choi, and K. W. Kim, "Compact ultra-wideband phase inverter using microstrip-CPW-slotline transitions," *Electronics*, Vol. 10, 252–258, 2021, doi: 10.3390/electronics10030252.
40. Weng, M. H., C. W. Hsu, S. W. Lan, and R. Y. Yang, "An ultra-wideband bandpass filter with a notch band and wide upper bandstop performances," *Electronics*, Vol. 8, 2019, doi: 10.3390/electronics8111316.
41. Moukala Mpele, P., F. Moukanda Mbango, D. B. O. Konditi, and F. Ndagijimana, "A novel quadband ultra miniaturized planar antenna with metallic vias and defected ground structure for portable devices," *Heliyon*, Vol. 7, e06373, 2021, doi: 10.1016/j.heliyon.2021.e06373.
42. Capet, N., C. Martel, J. Sokoloff, and O. Pascal, "Optimum high impedance surface configuration for mutual coupling reduction in small antenna arrays," *Progress In Electromagnetics Research B*, Vol. 32, 283–297, 2011.
43. Sanabria, C., R. M. H. Gonzalez, and M. L. Aranda, "A simple model of inter-metallic connections (vias) in CMOS resonant rotary traveling wave oscillator (RTWO)," *Proceedings of the 2017 14th International Conference on Electrical Engineering, Computing Science and Automatic Control.*, 1–5, 2017, doi: 10.1109/ICEEE.2017.8108860.
44. Ji, C. H., F. Herrault, and M. G. Allen, "A metallic buried interconnect process for through-wafer interconnection," *Journal of Micromechanics and Microengineering*, Vol. 18, 2008, doi: 10.1088/0960-1317/18/8/085016.
45. Palanisamy, P. and M. Subramani, "Design of metallic via based octa-port UWB MIMO antenna for iot applications," *IETE Journal of Research*, 1–11, 2021, doi: 10.1080/03772063.2021.1892540.
46. Moitra, S., R. Dey, and P. S. Bhowmik, "Design and band coalition of dual band microstrip filter using DGS, coupled line structures and series inductive metallic vias," *Proceedings of the Analog Integrated Circuits and Signal Processing*, Vol. 101, 77–88, Springer US, 2019, doi: 10.1007/s10470-019-01412-2.
47. Wadood, M. Y. and F. Babaeian, "A compact via-less ultra-wideband microstrip filter by utilizing open-circuit quarter wavelength stubs," *Int. Scholary and Scientific Research* & *Innovation*, Vol. 13, 178–181, 2019.
48. Zhang, R. and L. Zhu, "Design of a wideband bandpass filter with composite short-and open-circuited stubs," *IEEE Microwave and Wireless Components Letters*, Vol. 24, 96–98, 2014, doi: 10.1109/LMWC.2013.2291197.
49. Collin, R. E., *Foundations for Microwave Engineering*, D. G. Dudley, Ed., 2nd Edition, John Wiley & Sons, Inc., New York, 2001, doi: 10.1049/ep.1967.0023.
50. Mumford, W. W., "Maximally-flat filters in waveguide," *Bell System Technical Journal*, Vol. 27, 684–713, 1948, doi: 10.1002/j.1538-7305.1948.tb00919.x.
51. Chen, T. S., "Waveguide resonant-iris filters with very wide passband and stopbands," *International Journal of Electronics*, Vol. 21, 401–424, 1966, doi: 10.1080/00207216608937922.
52. Lu, H., J. Huang, X. Zhang, and N. Yuan, "Compact dual-band microstrip bandpass filter using stub-loaded stepped-impedance resonator," *Proceedings of the Advanced Information Technology, Electronic and Automation Control Conference (IAEAC)*, 1494–1498, 2017, doi: 10.1109/IAEAC.2017.8054262.
53. Wang, H., L. Zhu, and W. Menzel, "Ultra-wideband bandpass filter with hybrid microstrip/CPW structure," *IEEE Microwave and Wireless Components Letters*, Vol. 15, 844–846, 2005, doi: 10.1109/LMWC.2005.860016.
54. Moukanda Mbango, F., F. Ndagijimana, and A. L. Lomanga Okana, "Dual coaxial probes in transmission inserted by dielectric with two different thicknesses to extract the material complex relative permittivity: Discontinuity impacts," *Progress In Electromagnetics Research C*, Vol. 110, 67–80, 2021, doi: 10.2528/PIERC21010403.
55. Killamsetty, V. K. and B. Mukherjee, "Compact triple band bandpass filters design using mixed coupled resonators," *AEU — International Journal of Electronics and Communications*, Vol. 107, 49–56, 2019, doi: 10.1016/j.aeue.2019.03.005.

56. Denis, B., K. Song, and F. Zhang, "Compact dual-band bandpass filter using open stub-loaded stepped impedance resonator with cross-slots," *International Journal of Microwave and Wireless Technologies*, Vol. 9, 269–274, 2017, doi: 10.1017/S1759078715001786.
57. Malherbe, J. A. G., "Application of a series open circuit stub transform to bandpass filter design," *2018 48th European Microwave Conference, EuMC 2018*, 368–371, 2018, doi: 10.23919/EuMC.2018.8541510.
58. Kusama, Y. and R. Isozaki, "Compact and broadband microstrip band-stop filters with single rectangular stubs," *Applied Sciences*, Vol. 9, 248–259, 2019, doi: 10.3390/app9020248.
59. Talluri, S. R., "Design of dual band-reject filter based on short-circuited parallel coupled lines structure at S-band," *International Journal of Advances in Microwave Technology*, Vol. 3, 180–184, 2018, doi: 10.32452/ijamt.2018.180184.
60. Ramanujam, P., C. Arumugam, P. G. R. Venkatesan, and M. Ponnusamy, "Design of compact UWB filter using parallel-coupled line and circular open-circuited stubs," *IETE Journal of Research*, Vol. 0, 1–8, 2020, doi: 10.1080/03772063.2020.1803772.
61. Boutejdar, A., G. Nadim, and A. S. Omar, "Compact bandpass filter structure using an open stub quarter-wavelength microstrip line corrections," *Proceedings of the 35th European Microwave Conference*, Vol. 2, 1271–1273, 2005, doi: 10.1109/EUMC.2005.1610166.
62. David, M., "Pozar microwave filters," *Microwave Engineering*, 71–73, Wiley & Sons Ltd., USA, 2012.
63. Edwards, T. C. and M. B. Steer, *Foundations for Microstrip Circuit Design*, 4th Edition, John Wiley & Sons, Ltd., Chichester, UK, 2016, doi: 10.1002/9781118936160.
64. Moukanda Mbango, F. and F. Ndagijimana, "Electric parameter extractions using a broadband technique from coaxial line discontinuities," *International Journal of Scientific Research and Management*, Vol. 7, 248–253, 2019, doi: 10.18535/ijsrm/v7i5.ec01.
65. Bird, T. S., "Definition and misuse of return loss," *IEEE Antennas and Propagation Magazine*, Vol. 51, 166–167, 2009, doi: 10.1109/MAP.2009.5162049.
66. Fischer, B. E., V. Way, A. Arbor, I. J. Lahaie, V. Way, and A Arbor, "On the definition of return loss," *IEEE Antennas and Propagation Magazine*, Vol. 55, 172–174, 2013, doi: 10.1109/MAP.2013.6529339.
67. Beatty, R. W., "Insertion loss," *Proceedings of the IEEE*, Vol. 52, 663–671, 1964, doi: 10.1109/PROC.1964.3047.